



Grain boundary configurational entropy: a challenge

Pavel Lejček^{1,2,*}  and Andrea Školáková¹

¹Institute of Physics, Czech Academy of Sciences, Na Slovance 2, 182 21 Prague 8, Czech Republic

²Central European Institute of Technology, CEITEC BUT, Brno University of Technology, Purkyňova 123, 612 69 Brno, Czech Republic

Received: 17 April 2023

Accepted: 24 May 2023

Published online:

12 June 2023

© The Author(s) 2023

ABSTRACT

While the bulk of the high-entropy alloys is widely studied and characterized by their configurational entropy, there is a lack of general information regarding the configurational entropy of the grain boundaries. Here, we derived for the first time the basic relationships of this thermodynamic quantity related to the solute segregation at grain boundaries. Some examples of the appearance of the grain boundary configurational entropy are shown, and its effect on intergranular properties is discussed. It is stated that the role of grain boundary configurational entropy in interfacial properties is not completely clear and represents a challenge for future research.

Introduction

One of the new, dynamically developing fields of materials science, is complex concentrated systems, also called high-entropy alloys (HEAs) [1]. The concept of HEAs containing 5 or more principal elements has attracted scientific attention since Cantor [1] and Yeh [2] published their influential papers independently of each other. It is generally claimed that such complex concentrated systems exhibit high configurational entropy of the random mixing of elements leading to the formation of simple solid solutions or their mixture and preventing the formation of intermetallic phases. Therefore, the tendency for the formation of any clusters or precipitation of phases is lowered [3]. The value of configurational entropy thus mainly affects the stability of phases [4].

However, it is widely shown that the presence of intermetallic phases is highly likely [5–8]. In work [7] was shown that the formation of intermetallic phases is possible only at an intermediate temperature range. Such temperature range affects the role of entropy which starts to lose dominance and the formation of intermetallic phases is favored and triggered due to sufficient diffusion. The crystallographic structures of solid solutions are simple fcc [1, 9], bcc [10–12], and hcp [13, 14] types depending on the chemical composition of HEAs. The solid solutions are kinetically stable due to the sluggish diffusion of atoms; thereby, the possible precipitation of intermetallic phases is also suppressed. HEAs have become studied intensively due to their unique microstructure, phase composition, and mainly adjustable properties, and opened new possibilities and strategies in advanced alloy design. Among the

Handling Editor: P. Nash.

Address correspondence to E-mail: lejcekp@fzu.cz

exceptional properties belong high strength, hardness, excellent wear resistance and high-temperature strength, structure stability, and corrosion and oxidation resistance [15].

As was mentioned above, one of the general characteristics of these materials is the high value of the configurational entropy which seems to be responsible for the exceptional properties of the HEAs. However, the configurational entropy can also be applied to the grain boundaries. Recently, a concept of high-entropy grain boundaries was proposed [16, 17]. The main advantage of these grain boundaries whose composition is affected by solute segregation, is high value of the configurational entropy which may become origin of exceptional properties such as suppression of interfacial precipitation and stabilization of nanocrystalline structures [16, 18].

Nevertheless, it was argued in [19] that high mixing entropy may not be sufficient to prevent the segregation of the elements, although other authors claimed the opposite [2]. Grain boundaries generally act as barriers for the motion of dislocations resulting in the enhancing of the strength or hardness of alloys. This strengthening could be reduced at the intermediate temperatures as the boundaries are weakened by the segregation of solutes and/or impurities [20]. On the other hand, the ductility of alloys tested at high temperatures increased thanks to the easy motion of the boundaries. The pure metals with fcc structure as well as the alloys with low stacking fault energy (SFE) exhibit high ductility in a wide temperature range. The opposite trend could be observed in the case of the most studied HEAs, specifically Cantor alloy with equimolar chemical composition CoNiFeCrMn. As mentioned above, the ductility decreased at higher temperatures, especially at the intermediate temperatures [21], although the alloy is single fcc-phase solid solution, as well. This was attributed to the nanosegregation of one of the Ni, Cr, and Mn which resulted in the decohesion of the grain boundary [22, 23]. Schuh et al. [24] emphasized that strengthening cannot be exclusively explained only by the consideration of solute segregation at grain boundaries. Further, the segregation could also negatively influence the initial stage of corrosion. The dissolution of Cantor alloy is accelerated when the Cr-enriched phases form due to the ongoing microsegregation [25]. However, grain boundary segregation and grain boundary engineering have not been studied and developed extensively in the

case of HEAs so far. Therefore, there is a substantial lack of information. One of the unsolved fundamental problems in this respect is the relationship between the configurational entropy and the thermodynamic characteristics of grain boundary segregation.

In this context, a general question arises what the configurational entropy of the grain boundaries is itself, and how is related to that of the bulk material as well as to the characteristics of the solute segregation not only in HEAs but also in diluted systems. This topic is discussed in this paper for the first time.

Thermodynamic fundamentals

The total configurational entropy, ${}^T S^{\text{conf}}$ (in J K^{-1}), in an n -component real system is defined as

$${}^T S^{\text{conf}} = \sum_i^n n_i S_i^{0, \text{conf}} = -R \sum_i^n n_i \ln X_i, \quad (1)$$

where n_i and X_i are the number of moles and the mole fractions in the alloy, respectively, of component i , $S_i^{0, \text{conf}}$ (in $\text{J mol}^{-1} \text{K}^{-1}$) is the molar entropy of component i , and $R = 8.3141 \text{ J mol}^{-1} \text{K}^{-1}$ is the universal gas constant [26]. It is worth noting that the configurational entropy differs from the real mixing entropy, defined as

$${}^T S^{\text{mix}} = \sum_i^n n_i \bar{S}_i = \frac{{}^T H^{\text{mix}}}{T} - R \sum_i^n n_i \ln a_i, \quad (2)$$

where $a_i = \gamma_i X_i$ is the activity of component i in the alloy, γ_i is the activity coefficient of component i , ${}^T H^{\text{mix}}$ (kJ mol^{-1}), is the total mixing enthalpy and \bar{S}_i is the partial molar entropy of component i [26].

Equation (1) can also be rewritten to express the molar configurational entropy as

$$S^{\text{conf}} = \sum_i^n X_i S_i^{0, \text{conf}} = -R \sum_i^n X_i \ln X_i, \quad (3)$$

Besides their application to the bulk, expressions (1) and (2) can also be applied to the grain boundary (GB),

$$S_{\text{GB}}^{\text{conf}} = \sum_i^n X_i^{\text{GB}} S_i^{0, \text{conf, GB}} = -R \sum_i^n X_i^{\text{GB}} \ln X_i^{\text{GB}}, \quad (4)$$

where the index GB relates the variable to the grain boundary. Accepting

$$X_M^{GB} = 1 - \sum_i^{i \neq M} X_i^{GB}, \tag{5}$$

where M is the host component, we can rewrite Eq. (4) as

$$S_{GB}^{conf} = -R \left(\sum_i^{i \neq M} X_i^{GB} \ln \frac{X_i^{GB}}{X_M^{GB}} + \ln X_M^{GB} \right). \tag{6}$$

In contrast to S^{conf} , the grain boundary configurational entropy, S_{GB}^{conf} , is temperature dependent as the grain boundary concentrations change substantially with temperature due to the segregation effects which reflect the minimization of the Gibbs energy of the system. Under some assumptions (segregation of all solutes at the substitutional sites, full coverage of the grain boundaries by all solutes, monolayer segregation), the general segregation isotherm of the Langmuir–McLean type for a real system can be written as [27]

$$\frac{a_I^{GB}}{a_M^{GB}} = \frac{a_I}{a_M} \exp\left(-\frac{\Delta G_I^0}{RT}\right). \tag{7}$$

Alternatively,

$$\frac{X_I^{GB}}{1 - \sum_{j \neq M} X_j^{GB}} = \frac{X_I}{1 - \sum_{j \neq M} X_j} \exp\left(-\frac{\Delta G_I}{RT}\right), \tag{8a}$$

i.e.,

$$X_I^{GB} = \frac{X_I \exp(-\Delta G_I/RT)}{1 - \sum_{j \neq M} X_j [1 - \exp(-\Delta G_j/RT)]}, \tag{8b}$$

In Eq. (7),

$$\Delta G_I^0 = \Delta H_I^0 - T \Delta S_I^0, \tag{9}$$

T (K) is the temperature, ΔG_I^0 is the standard (ideal) Gibbs energy of segregation of solute I at the grain boundaries, composed of the standard enthalpy of grain boundary segregation, ΔH_I^0 , and the standard entropy of grain boundary segregation, ΔS_I^0 . In Eqs. (8a) and (8b),

$$\Delta G_I = \Delta H_I - T \Delta S_I = \Delta G_I^0 + \Delta G_I^E. \tag{10}$$

In Eq. (10), ΔH_I and ΔS_I are the enthalpy and entropy of segregation, respectively, in a real system. ΔG_I^E is the excess Gibbs energy of segregation representing the difference between the Gibbs energy of segregation and the standard Gibbs energy of segregation [27]. Its value is hardly measurable and

therefore, it is frequently estimated using the binary (Fowler) and ternary (Guttman) interaction coefficients [27, 28]. As Eq. (8b) is identical with the Butler equation [29] if $\Delta G_I = \exp[\omega(\sigma_I^0 - \sigma_M^0)/RT]$, where ω is the molar grain boundary area and $\sigma_{I,M}^0$ are the molar energies of the components I and M . Nevertheless, the nature of ΔG_I can further be extended based on, e.g., extended Butler equation [29, 30] and Wynblatt model [28, 31]. As the nature of ΔG_I is not primarily important in the relationship with grain boundary configurational entropy, we will consider it here only in the sense of Eq. (10). To get primary insight into the relationship between the configurational entropy and the grain boundary segregation, we will consider a binary system for simplicity.

As follows from Eq. (2), the partial molar entropy of component i in a binary alloy can be expressed as

$$S_i^{conf} = \left(\frac{\partial^T S^{conf}}{\partial n_i} \right)_{T, n_j} = -R \ln X_i. \tag{11}$$

This expression is valid for both the bulk and the grain boundary GB , as well as for solutes i and host metal M . Consequently, we can adopt Eq. (6) for an ideal binary system to get

$$\frac{\exp\left[-\left(S_I^{conf, GB} - S_M^{conf, GB}\right)/R\right]}{\exp\left[-\left(S_I^{conf} - S_M^{conf}\right)/R\right]} = \exp\left(-\frac{\Delta G_I}{RT}\right), \tag{12}$$

i.e.,

$$\begin{aligned} & \left(S_I^{conf, GB} - S_M^{conf, GB} \right) - \left(S_I^{conf} - S_M^{conf} \right) \\ &= \left(\frac{\partial S_{GB}^{conf}}{\partial X_I^{GB}} \right)_T - \left(\frac{\partial S^{conf}}{\partial X_I} \right)_T = \frac{\Delta G_I}{T} = \frac{\Delta H_I}{T} - \Delta S_I \\ &= \frac{\Delta H_I^0}{T} - \Delta S_I^0 + \frac{\Delta G_I^E}{T}. \end{aligned} \tag{13}$$

Differentiation of S_{GB}^{conf} for binary alloy (Eq. (6)) by X_I^{GB} at constant temperature results in

$$\left(\frac{\partial S_{GB}^{conf}}{\partial X_I^{GB}} \right)_T = -R \ln \frac{X_I^{GB}}{1 - X_I^{GB}} = -R \left(\ln \frac{X_I}{1 - X_I} - \frac{\Delta G_I}{RT} \right), \tag{14}$$

and differentiation by T provides

$$\frac{dS_{GB}^{conf}}{dT} = X_I^{GB} (1 - X_I^{GB}) \frac{\Delta H_I^0 + \Delta G_I^E - d\Delta G_I^E/dT}{RT^2}. \tag{15}$$

Using Eqs. (6) and (8b), we get

$$S_{\text{GB}}^{\text{conf}} = -R \frac{\sum_{j \neq M} X_j \exp(-\Delta G_j/RT) \left[\ln \left(X_j / \left(1 - \sum_{j \neq M} X_j \right) \right) - \Delta G_j/RT \right]}{1 - \sum_{j \neq M} X_j [1 - \exp(\Delta G_j/RT)]} \quad (16)$$

Equation (16) provides the direct relationship between the segregation quantities and the configurational entropy in a real system.

In principle, we can also apply more sophisticated approaches to describe the segregation isotherms, e.g., for multilayer segregation based on the BET (Brunauer–Emmett–Teller) approach [32].

Up to now, we treated the problem from the viewpoint of averaged grain boundary composition and corresponding averaged (= effective) thermodynamic quantities. However, theoretical calculations provide us with the energy of solute segregation for individual grain boundary sites which might result in the concentrations at these sites. To refine the above relationships, we can rewrite Eq. (8b) according to the White and Coghlan model [33] for a single grain boundary as

$$X_I^{\text{GB}} = \sum_k^N \zeta_k X_{I,k}^{\text{GB}} = \sum_k^N \zeta_k \frac{X_I \exp(-\Delta G_{I,k}/RT)}{1 - \sum_{j \neq M} X_j [1 - \exp(-\Delta G_{j,k}/RT)]}, \quad (17)$$

with ζ_k being a weight factor for individual grain boundary sites fulfilling the condition $\sum_k^N \zeta_k = 1$ and N being the number of grain boundary sites. Accordingly,

$$S_{\text{GB}}^{\text{conf}} = -R \sum_k^N \zeta_k \left(\sum_k^N X_{k,i}^{\text{GB}} \ln X_{k,i}^{\text{GB}} \right). \quad (18)$$

Under some assumptions, we can consider the segregation energy as a combination of the segregation energies of sites k , $\Delta E_{I,k}$, [34]

$$\Delta E_I = \sum_{k=1}^N \zeta_k \Delta E_{I,k}. \quad (19)$$

Analogous expressions will hold for the other thermodynamic quantities of grain boundary segregation. Then, the above given formulas can be refined by using Eqs. (17)–(19). For simplicity, we will deal here with the averaged quantities. A further reason is that we do not have representative data calculated for

individual grain boundary sites in complex multi-component systems.

Relations between configurational entropy and grain boundary segregation

Note to high-entropy alloys

It is evident from Eq. (14) that the maximum grain boundary configurational entropy in a binary alloy is obtained for its equimolar composition. It is worth noting that the condition of maximum configurational entropy also holds for equimolar composition in an n -component alloy. Due to the similarity of Eqs. (3) and (4), the same conclusion is also drawn for the equimolar crystal bulk supposing it represents the homogeneous solid solution.

This result has an important consequence. If we have, e.g., 5-component single phase alloy with equimolar bulk composition (i.e., atomic concentration of each solute is 0.2), then $S^{\text{conf}} = 1.609 R$. However, after annealing the solutes segregate to the grain boundary and thus, the composition of the grain boundary is no longer equimolar. An example representing this situation in a nearly equimolar FeMnNiCoCr alloy after annealing at 450 °C for various time periods [35] is given in Table 1.

It is apparent that this annealing results in gradual solute segregation and consequently, in the reduction of the configurational entropy. In all cases, its values are lower than that in the bulk and it loses the character of a HEA region if $S_{\text{GB}}^{\text{conf}} < 1.5 R$ [36]. This situation can also be interpreted as an ordering of the grain boundary. In fact, this is a common feature of the HEAs.

However, in the quinary system Fe–Mn–Ni–Co–Cr with non-equimolar compositions, we can find conditions for reaching a maximum grain boundary

Table 1 Grain boundary composition (at%) of a quinary alloy [35]

	Fe	Mn	Ni	Co	Cr	S^{conf}/R
Bulk	18.9	19.9	20.6	20.1	20.5	1.609
GB 450 °C/6 h	15	25	34	15	11	1.525
GB 450 °C/18 h	2	38	53	4	3	1.016
GB 450 °C/48 h	1	41	54	3	1	0.896

configurational entropy of $1.609 R$. Accepting for simplicity a very rough assumption of the ideality of this system and accepting the values of the Gibbs energy of segregation in bcc iron at 800 K to be -3.8 kJ mol^{-1} for Co, -5.6 kJ mol^{-1} for Cr, -6.6 kJ mol^{-1} for Mn, and -6.6 kJ mol^{-1} for Ni (the absolute values of the Fowler coefficients are less than 3 kJ mol^{-1}) [28], the equimolar composition of a general grain boundary and thus $S_{\text{GB}}^{\text{conf}} = 1.609 R$ can be obtained for the bulk composition of this alloy being 9 at% Fe, 16 at% Co, 25 at% Cr, 25 at% Ni and 25 at% Mn exhibiting $S^{\text{conf}} = 1.550 R$. Similarly, the maximum value of the grain boundary configurational entropy can be reached for slightly tuned bulk composition at different temperatures.

Dilute binary alloys

An opposite situation occurs in the case of grain boundary segregation in dilute alloys. Here, the composition of the grain boundaries is characterized by increased solute concentration and reduction of the concentration of the host metal. This fact contributes to an increase in the grain boundary configurational entropy compared to that of the bulk. We can demonstrate it by the example of diluted Fe–P alloys.

The grain boundary segregation in P-doped bcc iron-based alloys has been studied rather frequently since the pioneering quantitative work of Erhart and Grabke on polycrystalline Fe–P-based alloys [37]. The measurements of its segregation in polycrystalline materials [37] as well as in well-characterized bicrystals [38] resulted in the evaluation of the segregation enthalpies and entropies [28]. Using the data for phosphorus segregation at a general boundary which is most frequently present in typical polycrystalline materials, $\Delta H_p^0 = -39 \text{ kJ mol}^{-1}$ and $\Delta S_p^0 = +13 \text{ J mol}^{-1} \text{ K}^{-1}$, we did calculate the grain boundary concentrations at a temperature range 700–1100 K for three bulk concentrations, 0.1, 0.3, and 0.5 at% using Eq. (8b) with accounting for P–P interaction in Fe, $\alpha_{\text{P(Fe)}} = +4.5 \text{ kJ mol}^{-1}$, and maximum grain boundary coverage $X^0 = 2/3$ [28]. These data together with the values of the grain boundary configurational entropy are listed in Table 2 and shown in Fig. 1.

As mentioned above, the condition for maximum configurational entropy, $X_p^{\text{GB}} = 0.5$, depends on the

temperature and bulk composition of the alloy. This composition of the grain boundaries is reached at lower temperatures in the case of lower bulk concentrations compared to higher ones. Using Eq. (9), we may derive the value of the temperature, T^{MAX} , of maximum configurational entropy, $0.693 R$, for the equimolar composition of the grain boundary. For an ideal binary system, we can write

$$1 = \frac{X_I}{1 - X_I} \exp\left(-\frac{\Delta G_I}{RT^{\text{MAX}}}\right), \tag{20}$$

and thus

$$\ln \frac{X_I}{1 - X_I} = \frac{\Delta G_I}{RT^{\text{MAX}}} = \frac{\Delta H_I^0}{RT^{\text{MAX}}} - \frac{\Delta S_I^0}{R} + \frac{\Delta G_I^E}{RT^{\text{MAX}}} \tag{21}$$

i.e.,

$$T^{\text{MAX}} = \frac{\Delta H_I^0 + \Delta G_I^E}{R \ln[X_I/(1 - X_I)] + \Delta S_I^0}. \tag{22}$$

It is evident that the temperature at which the maximum configurational entropy (T^{MAX}) is reached, increases with increasing the bulk concentration of the solute (Fig. 2),

Table 2 Grain boundary concentrations of phosphorus (at%) at a general grain boundary in an Fe–P alloy containing 0.01, 0.03, and 0.05 at% P, and corresponding values of $S_{\text{GB}}^{\text{conf}}/R$. The values of S^{conf}/R for the bulk of individual alloys are listed in the right column

X_p	T (K)	X_p^{GB}	$S_{\text{GB}}^{\text{conf}}/R$	S^{conf}/R
0.001	700	0.530	0.691	0.0079
	800	0.418	0.680	
	900	0.313	0.621	
	1000	0.223	0.531	
	1100	0.169	0.454	
0.003	700	0.614	0.667	0.0204
	800	0.556	0.687	
	900	0.483	0.693	
	1000	0.406	0.675	
	1100	0.333	0.636	
0.005	700	0.634	0.657	0.0315
	800	0.596	0.675	
	900	0.543	0.689	
	1000	0.482	0.692	
	1100	0.414	0.678	

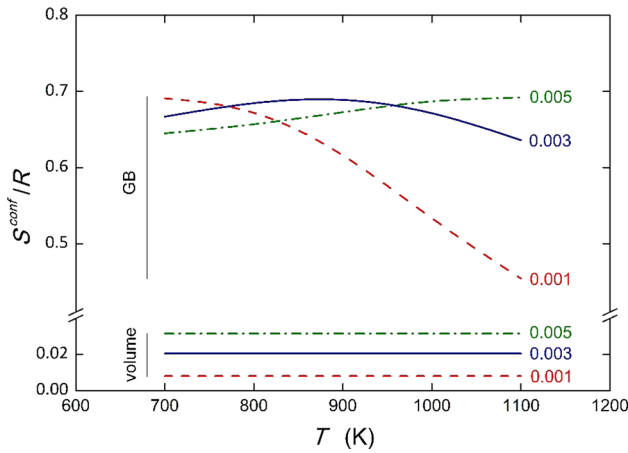


Figure 1 Temperature dependence of the configurational entropy for grain boundary and bulk in Fe–P systems with various bulk concentrations of P (denoted by the values in the figure).

$$\frac{\partial T^{MAX}}{\partial X_I} = -R \frac{(T^{MAX})^2}{\Delta H_I^0 + \Delta G_I^E X_I(1 - X_I)} > 0, \quad (23)$$

with decreasing the value of the segregation enthalpy (i.e., increasing the absolute value of ΔH_I^0) (Fig. 3a),

$$\frac{\partial T^{MAX}}{\partial \Delta H_I^0} = \frac{T^{MAX}}{\Delta H_I^0 + \Delta G_I^E} < 0, \quad (24)$$

and with decreasing the value of the segregation entropy (Fig. 3b),

$$\frac{\partial T^{MAX}}{\partial \Delta S_I^0} = -\frac{(T^{MAX})^2}{\Delta H_I^0 + \Delta G_I^E} > 0. \quad (25)$$

Let us mention that in inequalities (23)–(25), $|\Delta H_I^0| > |\Delta G_I^E| = 2|\alpha_{I(M)}|X_I^{GB}$, where $\alpha_{I(M)}$ is the

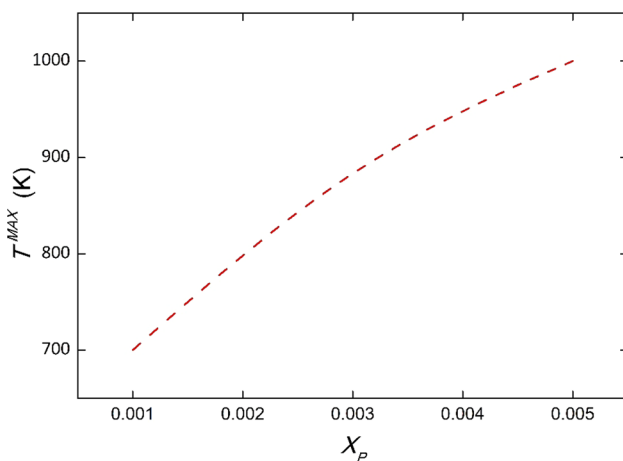


Figure 2 Dependence of T^{MAX} for Fe–P alloys with varied bulk concentrations of phosphorus, X_P .

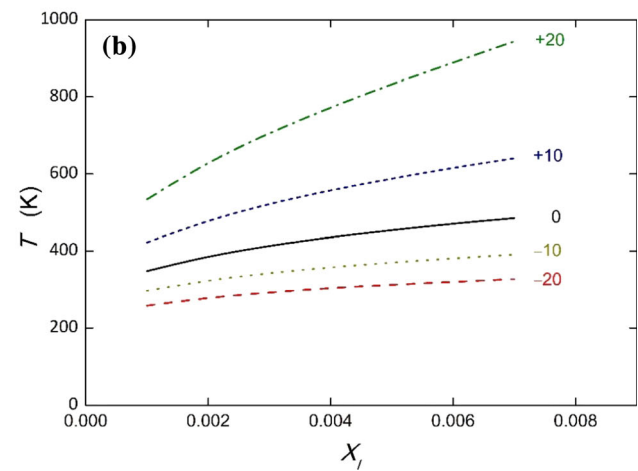
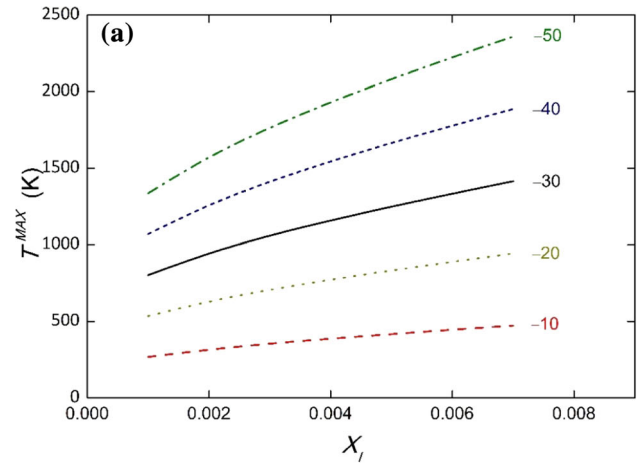


Figure 3 Model dependence of the temperature of maximum configurational entropy, T^{MAX} , for varied bulk concentrations of a solute, X_I . **a** for varied segregation enthalpy (represented by the data in kJ mol^{-1}); **b** for varied segregation entropy (represented by the data in $\text{J mol}^{-1} \text{K}^{-1}$).

Fowler coefficient [28], Further, according to Eq. (19), the above formulas are also valid if the segregation quantities are considered for individual sites and Figs. 2 and 3 remain the same if these quantities are averaged according to Eq. (19).

It is also worth noting that S_{GB}^{conf} possesses the same value in binary alloys with interchanged values of X_I^{GB} and X_M^{GB} . Then we must keep in mind that we consider two cases, segregation of I in M and segregation of M in I . due to different values of ΔG_I and ΔG_M . The same values of S_{GB}^{conf} are then obtained for different values of bulk concentrations of particular systems (cf. Eq. (16)).

High-entropy grain boundaries

As the maximum value of the configurational entropy of a considered equimolar HEA increases with the increasing number of components, $S^{\text{conf}} = R \ln n$, the value of $S_{\text{GB}}^{\text{conf}}$ can reach the values corresponding to those, which are characteristic for HEAs even in more diluted non-HEAs. For a simple example, a maximum value $S_{\text{GB}}^{\text{conf}} = 1.099R$ should be reached for a ternary system Fe–17 at% Cr–0.7 at% P at 800 K as estimated using the values $\Delta H_p^0 = -39 \text{ kJ mol}^{-1}$, $\Delta S_p^0 = +13 \text{ J mol}^{-1} \text{ K}^{-1}$, $\alpha_{\text{P(Fe)}} = +4.5 \text{ kJ mol}^{-1}$, $X^0 = 2/3$, $\Delta H_{\text{Cr}}^0 = -12 \text{ kJ mol}^{-1}$, $\Delta S_{\text{Cr}}^0 = -8 \text{ J mol}^{-1} \text{ K}^{-1}$, $\alpha_{\text{Cr(Fe)}} = +1.1 \text{ kJ mol}^{-1}$, $X^0 = 1$ [28], and $\alpha'_{\text{P-Cr(Fe)}} = -17 \text{ kJ mol}^{-1}$ [39]. It is worth noting that the value of the configurational entropy in the bulk is $S^{\text{conf}} = 0.446 R$, only. Although the value of $1.099 R$ does not correspond yet to the HEA condition, it is evident that the alloy composition and suitable temperature produce grain boundaries characterized by high entropy as was shown already in Part Note to high-entropy alloys.

Anisotropy of grain boundary configurational entropy

Much larger differences between the values of the configurational entropy for the grain boundary and the bulk can be obtained in the case of quaternary alloys. A systematic study of the temperature dependence of the grain boundary segregation in an Fe–3.55 at% Si alloy containing 0.0089 at% P and 0.014 at% C ($S^{\text{conf}} = 0.121 R$) using Auger electron spectroscopy [40] resulted in the evaluation of the averaged standard enthalpy and standard entropy of solute segregation at individual grain boundaries [41]. From the compositions of the grain boundaries, we can also determine the values of the grain

boundary configurational entropy. The grain boundary concentrations are listed in Table 3 and depicted in Fig. 4.

The values of $S_{\text{GB}}^{\text{conf}}$ are not so high as was shown in the previous example. This is because the concentrations of the solutes do not reach the equimolar composition at the grain boundary. However, the values of $S_{\text{GB}}^{\text{conf}}$ are still high enough compared to that of the bulk (cf. Figure 4): the maximum shown values are nearly by one order of magnitude higher than S^{conf} of the bulk. It only confirms the fact that in diluted alloys the grain boundary configurational entropy is higher than that in the bulk. Even here, the character of the anisotropy of S^{conf} remains identical when the concentrations and thermodynamic quantities considered for individual sites at the grain boundary are averaged according to Eqs. (17) and (19), respectively.

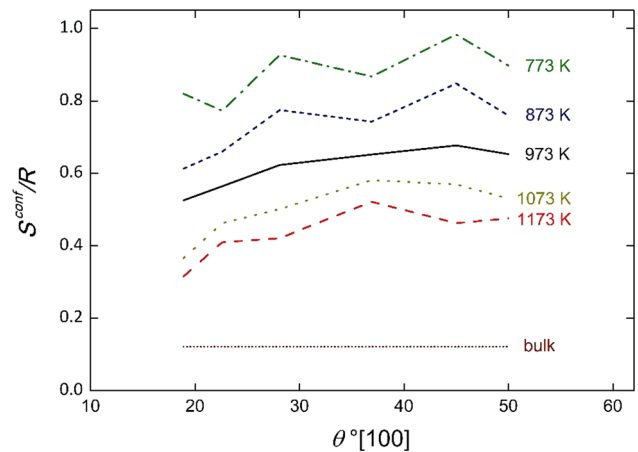


Figure 4 Orientation and temperature dependence of the configurational entropy at individual grain boundaries in bicrystals of and Fe–3.55 at% Si alloy containing 0.0089 at% P and 0.014 at% C. The horizontal line (bulk) represents the configurational entropy of the bulk.

Table 3 Concentrations of phosphorus, silicon, and carbon (at%) at individual grain boundaries of an Fe–Si–P–C alloy. The average standard error of the measured grain boundary concentrations is ± 0.5 at% for P, ± 1.0 at% for C, and ± 0.4 at% for Si [40]

T (K)	773			873			973			1073			1173		
	Si	P	C	Si	P	C	Si	P	C	Si	P	C	Si	P	C
{016}	4.1	4.3	19.4	2.5	4.3	10.1	3.6	3.4	6.0	2.5	2.3	3.2	2.3	1.9	2.4
{015}	2.2	7.8	14.4	2.4	6.9	9.2	2.5	6.1	5.9	2.4	5.1	3.5	2.4	4.6	2.4
{014}	1.1	13.3	20.8	3.2	7.3	13.2	3.7	5.6	7.2	3.9	3.6	4.6	3.8	2.7	3.1
{013}	1.0	13.6	16.2	1.5	11.8	9.7	1.9	10.0	6.6	2.1	8.9	4.6	2.5	7.7	3.1
{0kl}*	1.0	13.7	26.5	2.5	8.3	17.9	2.8	5.4	11.2	3.1	4.2	7.4	3.1	3.2	4.6
{0 7 15}	1.2	14.8	16.4	4.6	6.8	10.8	5.3	5.7	6.4	5.6	3.7	3.8	5.5	2.8	3.1

*45°[100] {0kl} is an incommensurate interface with irrational indices *k* and *l*

Nevertheless, there is another interesting finding. The orientation dependence of S_{GB}^{conf} follows the anisotropy of the absolute values of the segregation enthalpy [42] exhibiting minima at $22.6^\circ[100] \{015\}$ and $36.9^\circ[100] \{013\}$ special grain boundaries at 773 K (Fig. 4). However, it is apparent from Fig. 4 that the differences among the values of S_{GB}^{conf} of individual grain boundaries reduce and eventually reverse, thus exhibiting an opposite character of the anisotropy. This is also in agreement with the anisotropy of the values of the grain boundary concentrations [43] and was also observed in HEAs [44].

As shown previously [42], a specific relationship was found between the changes of the standard molar enthalpy and standard molar entropy, both of solute segregation at the grain boundaries, with changes in the grain boundary structure Ψ ,

$$\left(\frac{\partial \Delta H_I^0}{\partial \Psi}\right)_T / \left(\frac{\partial \Delta S_I^0}{\partial \Psi}\right)_T = T_{CE}, \quad (26)$$

which is called enthalpyentropy compensation effect, and T_{CE} is the compensation temperature. Accordingly,

$$\begin{aligned} \left(\frac{\partial \Delta G_I^0}{\partial \Psi}\right)_T &= \left(\frac{\partial \Delta H_I^0}{\partial \Psi}\right)_T \left(1 - \frac{T_{CE}}{T}\right) \\ &= \left(\frac{\partial \Delta H_I^0}{\partial \Psi}\right)_T \left(\frac{T - T_{CE}}{T}\right). \end{aligned} \quad (27)$$

It was concluded [42, 43] that the Gibbs energy of segregation is constant at T_{CE} (K) and independent of the grain boundary structure. This fact has a consequence that $(\partial \Delta G_I^0 / \partial \Psi)_T$ changes its sign and thus, the character of the anisotropy of grain boundary concentrations is reversed above and under T_{CE} .

As the grain boundary configurational entropy is composed of the grain boundary concentrations, we can expect similar dependence, which is also apparent from Fig. 4. To understand the changes of S_{GB}^{conf} , we will consider a binary ideal alloy for simplicity. In this case according to Eqs. (14) and (21)

$$\begin{aligned} \left(\frac{\partial S_{GB}^{conf}}{\partial \Psi}\right)_T &= -R \left[\ln \left(\frac{X_I}{1 - X_I} \right) - \frac{\Delta G_I^0}{RT} - \frac{1}{1 - X_I^{GB}} \right] \\ &\quad \left(\frac{\partial X_I^{GB}}{\partial \Psi}\right)_T - \frac{\Delta X_I^{GB}}{RT} \left(\frac{\partial \Delta G_I^0}{\partial \Psi}\right)_T. \end{aligned} \quad (28)$$

As

$$\left(\frac{\partial X_I^{GB}}{\partial \Psi}\right)_T = -X_I^{GB} (1 - X_I^{GB}) \frac{T - T_{CE}}{RT} \left(\frac{\partial \Delta H_I^0}{\partial \Psi}\right)_T, \quad (29)$$

using Eq. (27) we can write

$$\begin{aligned} \left(\frac{\partial S_{GB}^{conf}}{\partial \Psi}\right)_T &= X_I^{GB} \frac{T - T_{CE}}{RT} \left[(1 - X_I^{GB}) \left(\ln \frac{X_I}{1 - X_I} - \frac{\Delta G_I^0}{RT} \right) \right] \\ &\quad \left(\frac{\partial \Delta H_I^0}{\partial \Psi}\right)_T. \end{aligned} \quad (30)$$

If we accept

$$\begin{aligned} \eta(T) &= \frac{X_I^{GB}}{RT} \left[(1 - X_I^{GB}) \left(\ln \frac{X_I}{1 - X_I} - \frac{\Delta G_I^0}{RT} \right) \right] \\ &= \frac{X_I^{GB} (1 - X_I^{GB})}{RT} \ln \frac{X_I^{GB}}{1 - X_I^{GB}} < 0 \end{aligned} \quad (31)$$

for all temperatures and $X_I^{GB} < 0.5$. Then,

$$\left(\frac{\partial S_{GB}^{conf}}{\partial \Psi}\right)_T = \eta(T) (T - T_{CE}) \left(\frac{\partial \Delta H_I^0}{\partial \Psi}\right)_T. \quad (32)$$

It is apparent from Eq. (17) that the character of the anisotropy of ΔS_{GB}^{conf} reverses by crossing T_{CE} similarly to that of ΔG_I^0 and X_I^{GB} . This change is also apparent from Fig. 4.

It was established previously that the value of $T_{CE} = 900$ K [41] is the temperature at which the reversion occurs. However, it seems from Fig. 4 that the reversion of the anisotropy of S_{GB}^{conf} takes place at a slightly higher temperature. This discrepancy results from the simplification of the mathematical treatment applied to only an ideal binary system as the shift in T_{CE} can be affected by the real behavior of the system [45] characterized here mainly by strong repulsive interaction between Si and P atoms (Guttman ternary interaction parameter $\alpha'_{Si-P(Fe)} = -92$ kJ mol⁻¹) [46]. Despite the compensation temperature being the same for all mentioned solutes and grain boundaries, the compensation effect splits into two branches, one for phosphorus and carbon, and the other one for silicon [41]. This reflects in somehow diffuse transition and apparent shift of T_{CE} . However, Fig. 4 clearly demonstrates the reversed character of the anisotropy of S_{GB}^{conf} at temperatures above and under T_{CE} despite of the value of the compensation temperature.

Consequences of grain boundary configurational entropy and future perspectives

Materials properties are controlled by their Gibbs energy, G , and tend to reach the equilibrium characterized by a minimum of this thermodynamic quantity. The Gibbs energy of a system can be expressed as a combination of the ideal enthalpy, H_i^{id} , entropy, S_i^{id} , and mixing parameter, G^{mix} ,

$$\begin{aligned} G &= \sum_i X_i (H_i^{id} - TS_i^{id}) + \Delta G^{mix} \\ &= \sum_i X_i (H_i^{id} - TS_i^{id}) - TS^{conf} + \Delta G^E, \end{aligned} \quad (33)$$

where ΔG^E is the excess Gibbs energy of the alloy [26]. It is apparent that besides the configurational entropy, there are other entropic contributions such as vibrational, harmonic, anharmonic, and magnetic entropies which are included in the terms S_i^{id} . An expression analogous to Eq. (33) can be written for both the bulk and the grain boundary. Therefore, the properties of the material are affected by a synergistic influence of individual terms contributing to the total Gibbs energy of the system. However, here we will discuss the effect of one of these terms, i.e., of the grain boundary configurational entropy, despite that we are aware of the fact that observed behavior is not exclusively the result of the value of S_{GB}^{conf} .

It is widely accepted that entropy is a measure of the disorder of the system. In some cases, high entropy of grain boundaries can thus result in changing the structures of the grain boundaries up to an amorphous state [47]. The systems exhibiting high entropy may then exhibit exceptional properties [48]. If high configurational entropy results from solute segregation at grain boundaries, we may expect, for example, higher resistance to any type of clustering such as precipitation of second phases and intermetallic compounds [16]. It is also expected that the interfacial segregation will be reduced at lower temperatures in HEAs due to the opposite effects of the configurational entropy and driving force of the segregation process [49]. A similar effect might be expected in non-HEAs when the level of segregation induces high values of entropy. Maybe, it can also be connected to some tendency to short range ordering which has been observed in HEAs [50–52], and affecting, e.g., local distortion [50]. Consequently, the solid solubility of solutes increases at the grain

boundaries, compared to the bulk materials. This is evident from the data for P and C listed in Table 3 which are by 1–2 orders of magnitude higher than the solid solubility of these solutes in bcc iron. We can also find other examples in the literature, e.g., Bi in Cu [53] and In in Ni [54]. Additionally, we may reach such a composition of the grain boundaries exhibiting the configurational entropy on the level of HEAs, and occurring high-entropy grain boundaries can then serve as stabilizers of nanocrystalline structures [16]. Such segregated grain boundaries can also undergo various transitions in multicomponent alloys which can result in changed width of the grain boundaries and their structure [48].

Similarly, convoluted grain boundaries form in HEAs. However, in the case of equimolar HEAs, the segregated grain boundaries exhibit lower configurational entropy than the bulk. It is question, how does this fact reflect in the properties of the grain boundaries? In this respect, we can expect similar effects as in the case of the above-mentioned interfaces. Nevertheless, an impact is expected on, e.g., electrical, thermal, and ionic conductivities, the coercivity of magnets, and the stability of batteries as summarized in [48].

However, another question arises whether the behavior of the grain boundaries is primarily controlled by configurational entropy or by atomic bonds at the interface. It is known that a high concentration of phosphorus at the grain boundaries causes both the loss of intergranular cohesion [39] and an increase of the configurational entropy [55]. However, in the case of diluted systems with several segregating elements which compete for the sites but have different effects on the cohesion such as phosphorus and carbon in steels, the situation is rather complicated. For example, grain boundary segregation of phosphorus in Fe–Cr-based alloys increases with increasing content of chromium in the alloy while that of carbon is decreasing [55] (Table 4). In both these alloys, the values of S_{GB}^{conf} are nearly equal, but the alloys differ substantially in mechanical behavior as that with lower content of chromium possesses higher cohesion, while that with higher content of chromium exhibits intergranular brittle fracture [55].

This example suggests that chemical bonds play a dominant role in materials cohesion despite nearly identical values of the grain boundary configurational entropy.

Table 4 Composition of the grain boundaries (at%) in two Fe–Cr-based alloys containing 2.26 and 4.35 mass % Cr in

	Fe	P	C	O	Cr	S_{GB}^{conf}/R
2.26 mass % Cr alloy	68.73	13.60	8.12	6.25	3.30	1.019
4.35 mass % Cr alloy	64.13	17.64	7.49	3.28	7.46	1.091

In the case of grain boundary migration, the non-segregated grain boundaries exhibit a larger tendency to move than segregated grain boundaries [56, 57]. From the viewpoint of the configurational entropy, the non-segregated grain boundaries in HEAs possess lower S_{GB}^{conf} (comparable to that of the bulk) than segregated interfaces. On the other hand, the grain boundaries in highly segregated non-HEAs exhibit higher value of S_{GB}^{conf} compared to S^{conf} ; however, their motion is slower than that in relatively pure metals in both cases (e.g., [58–60]). It is apparent that the migration of the grain boundaries in all alloys is reduced due to a solute drag despite the value of the configurational entropy. Therefore, the effect of the grain boundary segregation and the formation of a solute atmosphere at the grain boundaries seems to affect dominantly the grain boundary migration.

The grain boundaries in nanocrystalline dilute alloys represent a special case. It is well known that grain boundary segregation can stabilize the nanocrystalline structures via inhibition of interfacial migration (see, e.g., [61, 62]). However, with decreasing the grain boundary size the volume of the grain boundaries increases and during solute segregation, the actual bulk concentration, X_I , decreases compared to the nominal (total) alloy concentration, X_I^T ,

$$X_I^T = fX_I^{GB} + (1-f)X_I \quad (34)$$

where f is the volume fraction of the grain boundaries [61]. For the simplest case of circular grains with the diameter d and grain boundary thickness h , both in nm, we can write [63]

$$f = 1 - \left(\frac{d-h}{d}\right)^3. \quad (35)$$

Supposing a general segregation isotherm of the Langmuir–McLean type with a single effective value of the Gibbs energy of segregation (Eq. (8a)), we get for a binary alloy,

$$X_I^{GB} = \frac{[1 + (f + X_I^T)(E-1)] \pm \sqrt{[1 + (f + X_I^T)(E-1)]^2 - 4fX_I^TE(E-1)}}{2f(E-1)}, \quad (36)$$

supposing $0 < X_I^{GB} < 1$. In Eq. (36), $E = \exp(-\Delta G_I/RT)$. We can now characterize the change of the configurational entropy with changing grain size for example of a binary Fe–0.005 at.% P using $h = 1$ nm, $\Delta H_P = -29$ kJ mol⁻¹, $\Delta S_P = +22$ J mol⁻¹ K⁻¹, $\alpha_{P(Fe)} = 4.5$ kJ mol⁻¹ [28], and thus, $\Delta G_P(800K) = -46$ kJ mol⁻¹. The corresponding dependence of S_{GB}^{conf} on the grain size is shown in Fig. 5. It is apparent from Fig. 5 that S_{GB}^{conf} decreases with decreasing grain size as the grain boundary concentration of the solute also decreases. This situation seems to be paradoxical as consequently, the effect of stabilization of the nanocrystalline structure due to grain boundary segregation fades and a lower value of S_{GB}^{conf} suggests better arrangement of the grain boundaries in nanocrystalline structures compared to large bicrystals. However, it may suggest that better arrangement of the grain boundaries in nanocrystals contributes to the reduction of grain boundary migration. Nevertheless, these paradoxes suggest that on the one hand, S_{GB}^{conf} itself is not decisive for the properties of the grain boundaries [64], but, on the other hand, its behavior still deserves sufficient attention.

Further, the self-diffusion of nickel is higher at grain boundaries of pure nickel compared to that in CoCrFeNi and CoCrFeMnNi HEAs exhibiting much

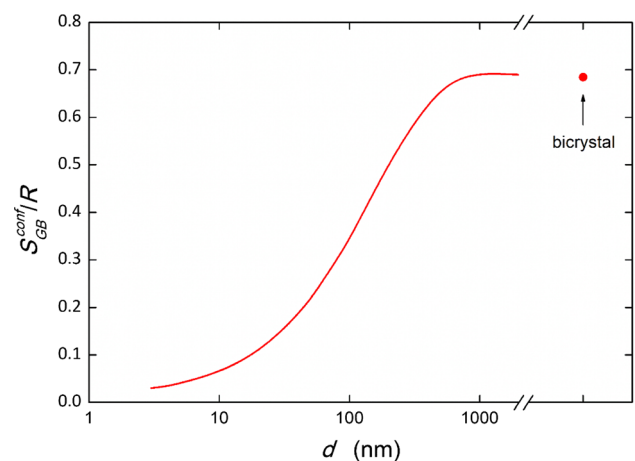


Figure 5 Change of the grain boundary configurational entropy with the grain size. Example data for a dilute Fe–P alloy (see the text for details).

higher S_{GB}^{conf} than the pure metal. Moreover, grain boundary diffusivity in the CoCrFeNi HEA is larger than that in CoCrFeMnNi one, however, at temperatures under 800 K, where the reversion occurs. It is supposed that the nature of added components and the character of their interaction play a more decisive role [65]. Another factor affecting the elemental segregation is the vacancy formation energy. The vacancy formation energy could be positive (e.g., Co, Fe, Ni) or negative (Cr). The negative vacancy formation energy indicates a thermodynamic drive for segregation resulting in the potential formation of the passive layer [66].

It seems that the configurational entropy plays an important role in the behavior of the grain boundaries due to the above-mentioned structural transitions [47] and for example, the solubility of the solutes at the grain boundaries is increased as we already mentioned above. The effect of disordering at the grain boundaries then competes with the chemistry and bond character. Nevertheless, there are still many unanswered questions. Some of them can be formulated as follows: What is the reason for the reversion of the diffusivity in the vicinity of 800 K? Is the enhanced solubility of solutes at the grain boundaries really a consequence of the higher configurational entropy and thus, the more open structure of grain boundaries? As there is a close relationship between the grain boundary configurational entropy and grain boundary segregation, does configurational entropy really play an inferior role? What is the role of the grain boundary configurational entropy in the enthalpy-entropy compensation effect? These and many other questions are still open providing a challenge in elucidating the effect of the grain boundary configurational entropy.

In this respect, we must add a comment. It is apparent from Eq. (16) that S_{GB}^{conf} is closely related to the characteristics of solute segregation at grain boundaries as well as to the bulk concentration of the solute. Both these variables determine the value of the grain boundary configurational entropy and control at which temperature the maximum value of S_{GB}^{conf} is reached. On the other hand, the value of S_{GB}^{conf} is determined simply by the grain boundary composition without considering the chemical nature of the system (Eq. (4)). This apparent contradiction—dependence only on numerical chemical composition in the latter case but the inclusion of the chemistry in

the former case—needs a deeper grasp and elaboration. Nevertheless, high value of S_{GB}^{conf} contributes substantially to the total molar Gibbs energy of the grain boundaries (cf. Eq. (33) for the grain boundary): The value of its product with temperature can reach 10 kJ mol^{-1} which is not negligible as compared to the values of the enthalpy and other entropy contributions. In this respect, it affects the behavior of the system apparently. In fact, the configurational energy is also closely related to the segregation energy. Supposing the Gibbs adsorption isotherm [27],

$$\Gamma_I^{GB} = -\frac{d\sigma^{GB}}{d\mu_I}, \tag{37}$$

where Γ_I^{GB} (in mol m^{-2}) is the grain boundary excess of component I , σ^{GB} is the grain boundary energy (in J m^{-2}) and μ_I is the bulk chemical potential of component I , and

$$d\sigma^{GB} = -\frac{1}{\omega} \left[\sum_i G_i^{0, GB} dX_i^{GB} + dG_{GB}^{conf} \right], \tag{38}$$

where $G_i^{0, GB}$ is the molar Gibbs energy of pure component i (in J mol^{-2}), we get in an ideal binary system,

$$dS_{GB}^{conf} = \frac{G_I^{0, GB} - G_M^{0, GB}}{T} dX_I^{GB} + (X_I^{GB} - X_I) d \ln X_I. \tag{39}$$

Similarly,

$$dS_{GB}^{conf} = (G_I^{0, GB} - G_M^{0, GB}) X_I^{GB} (1 - X_I^{GB}) \frac{\Delta H_I^0}{RT^3} dT. \tag{40}$$

By understanding this dialectic, the physical meaning of the role of the configurational entropy in various states and processes can be elucidated.

Due to the similarity with the grain boundaries, it is also evident that high-entropy surfaces will also exist. They should behave in very similar ways as the grain boundaries do [67] and all above derived expressions must also be valid for the surfaces in a qualitative way. We can also expect exceptional properties of high-entropy surfaces, mainly in the field of surface segregation and adsorption which can be reduced at lower temperatures as was mentioned above for the grain boundaries [49]. It is known that the materials with configurational entropy higher than $1.5 R$ exhibit a slower diffusion rate than normal

alloys, which implies higher resistance to high temperatures [68]. As the high configurational entropy impedes clustering, we may expect reduced tendencies to oxidation and corrosion of such surfaces. This can be further supported by ab initio simulations of oxidation and the chemical resistance of the basic material against these effects.

Conclusions

Configurational entropy is a thermodynamic quantity which is widely mentioned concerning high entropy alloys (HEAs) but has not been discussed generally for grain boundaries so far. It is shown that—in contrast to high-entropy alloys—it is larger in non-HEAs than that in the bulk due to the segregation effects. It is apparent that the grain boundary configurational entropy is closely related to grain boundary segregation. The basic expressions relating the grain boundary configurational entropy to the grain boundary segregation of solutes and/or impurities are derived, and the basic effects of individual variables are shown. Based on the experimental data, it is shown that the grain boundary configurational entropy exhibits pronounced anisotropy which is temperature dependent, and similarly to the segregation enthalpy, it is reversed by crossing the compensation temperature. Similarly to grain boundaries, high-entropy surfaces exist. Despite that it seems that the main effect of the configurational entropy is increased solubility of the solutes at the grain boundaries, while other effects such as interfacial segregation, migration, and diffusion, are controlled by the chemistry and bond character of the system, there are many non-answered questions suggesting that the phenomenon of the interfacial configurational entropy still represents a challenge to further research.

Acknowledgements

Financial support was provided by the Czech Science Foundation (Project No. GA-20-08130S) and by the Academy of Sciences of the Czech Republic (RVO:68378271).

Author contributions

PL contributed to the conceptualization, methodology, calculations, funding acquisition and writing—original draft. AŠ was involved in the conceptualization and writing—review and editing.

Funding

Open access publishing supported by the National Technical Library in Prague.

Data availability

There are no additional data. Detailed information can be provided by the corresponding author for request.

Declarations

Conflict of interest The authors declare that they have no known competing financial interests or personal relationships that could have appeared to influence the work reported in this paper.

Open Access This article is licensed under a Creative Commons Attribution 4.0 International License, which permits use, sharing, adaptation, distribution and reproduction in any medium or format, as long as you give appropriate credit to the original author(s) and the source, provide a link to the Creative Commons licence, and indicate if changes were made. The images or other third party material in this article are included in the article's Creative Commons licence, unless indicated otherwise in a credit line to the material. If material is not included in the article's Creative Commons licence and your intended use is not permitted by statutory regulation or exceeds the permitted use, you will need to obtain permission directly from the copyright holder. To view a copy of this licence, visit <http://creativecommons.org/licenses/by/4.0/>.

References

- [1] Cantor B, Chang ITH, Knight P, Vincent AJB (2004) Microstructural development in equiatomic multicomponent

- alloys. *Mater Sci Eng A* 375–377:213–218. <https://doi.org/10.1016/j.msea.2003.10.257>
- [2] Yeh JW, Chen SK, Lin SJ, Gan JY, Chin TS, Shun TT, Tsau CH, Chang SY (2004) Nanostructured high-entropy alloys with multiple principal elements: novel alloy design concepts and outcomes. *Adv Eng Mater* 6:299–303. <https://doi.org/10.1002/adem.200300567>
- [3] Nataraj CM, van de Walle A, Samanta A (2021) Temperature-dependent configurational entropy calculations for refractory high-entropy alloys. *J Phase Equilib Diffus* 42:571–577. <https://doi.org/10.1007/s11669-021-00879-9>
- [4] Biswas K, Kumar N (2020) The effect of configurational entropy of mixing on the design and development of novel materials. *Proc Indian Natl Sci Acad*. <https://doi.org/10.16943/ptinsa/2019/49674>
- [5] Schuh B, Völker B, Todt J, Schell N, Perrière L, Li J, Couzinié JP, Hohenwarter A (2018) Thermodynamic instability of a nanocrystalline, single-phase TiZrNbHfTa alloy and its impact on the mechanical properties. *Acta Mater* 142:201–212. <https://doi.org/10.1016/j.actamat.2017.09.035>
- [6] Wang YP, Li BS, Fu HZ (2009) Solid solution or intermetallics in a high-entropy alloy. *Adv Eng Mater* 11:641–644. <https://doi.org/10.1002/adem.200900057>
- [7] Chou TH, Huang JC, Yang CH, Lin SK, Nieh TG (2020) Consideration of kinetics on intermetallics formation in solid-solution high entropy alloys. *Acta Mater* 195:71–80. <https://doi.org/10.1016/j.actamat.2020.05.015>
- [8] Müller F, Gorr B, Christ H-J, Chen H, Kauffmann A, Laube S, Heilmaier M (2020) Formation of complex intermetallic phases in novel refractory high-entropy alloys NbMoCrTiAl and TaMoCrTiAl: Thermodynamic assessment and experimental validation. *J Alloys Compd* 842:155726. <https://doi.org/10.1016/j.jallcom.2020.155726>
- [9] Liu WH, He JY, Huang HL, Wang H, Lu ZP, Liu CT (2015) Effects of Nb additions on the microstructure and mechanical property of CoCrFeNi high-entropy alloys. *Intermetallics* 60:1–8. <https://doi.org/10.1016/j.intermet.2015.01.004>
- [10] Senkov ON, Scott JM, Senkova SV, Meisenkothen F, Miracle DB, Woodward CF (2012) Microstructure and elevated temperature properties of a refractory TaNbHfZrTi alloy. *J Mater Sci* 47:4062–4074. <https://doi.org/10.1007/s10853-012-6260-2>
- [11] Senkov ON, Wilks G, Scott J, Miracle DB (2011) Mechanical properties of Nb₂₅Mo₂₅Ta₂₅W₂₅ and V₂₀Nb₂₀Mo₂₀Ta₂₀W₂₀ refractory high entropy alloys. *Intermetallics* 19:698–706
- [12] Todai M, Nagase T, Hori T, Matsugaki A, Sekita A, Nakano T (2017) Novel TiNbTaZrMo high-entropy alloys for metallic biomaterials. *Scripta Mater* 129:65–68. <https://doi.org/10.1016/j.scriptamat.2016.10.028>
- [13] Zhao L, Zhang Z, Song Y, Liu S, Qi Y, Wang X, Wang Q, Cui C (2016) Mechanical properties and in vitro biodegradation of newly developed porous Zn scaffolds for biomedical applications. *Mater Des* 108:136–144. <https://doi.org/10.1016/j.matdes.2016.06.080>
- [14] Nagase T, Todai M, Nakano T (2020) Development of Ti–Zr–Hf–Y–La high-entropy alloys with dual hexagonal-close-packed structure. *Scripta Mater* 186:242–246. <https://doi.org/10.1016/j.scriptamat.2020.05.033>
- [15] Tsai M-H, Yeh J-W (2014) High-entropy alloys: a critical review. *Mater Res Lett* 2:107–123
- [16] Zhou N, Hu T, Luo J (2016) Grain boundary complexions in multicomponent alloys: challenges and opportunities. *Curr Opin Solid State Mater Sci* 20:268–277. <https://doi.org/10.1016/j.cossms.2016.05.001>
- [17] Luo J, Zhou N (2023) High-entropy grain boundaries. *Commun Mater* 4:7. <https://doi.org/10.1038/s43246-023-00335-w>
- [18] Kaptay G (2019) Thermodynamic stability of nano-grained alloys against grain coarsening and precipitation of macroscopic phases. *Metall Mater Trans A* 50:4931–4947. <https://doi.org/10.1007/s11661-019-05377-9>
- [19] Liu W, Wu Y, He J, Zhang Y, Liu C, Lu Z (2014) The phase competition and stability of high-entropy alloys. *JOM* 66:1973–1983. <https://doi.org/10.1007/s11837-014-1119-4>
- [20] Li W, Xie D, Li D, Zhang Y, Gao Y, Liaw PK (2021) Mechanical behavior of high-entropy alloys. *Progr Mater Sci* 118:100777. <https://doi.org/10.1016/j.pmatsci.2021.100777>
- [21] Diao H, Xie X, Sun F, Dahmen KA, Liaw PK (2016) Mechanical properties of high-entropy alloys. In: Gao MC, Yeh JW, Liaw PK, Zhang Y (ed) *High-entropy alloys: fundamentals and applications*, pp 181–236
- [22] Ming K, Li L, Li Z, Bi X, Wang J (2019) Grain boundary decohesion by nanoclustering Ni and Cr separately in CrMnFeCoNi high-entropy alloys. *Sci Adv* 5:eaay0639. <https://doi.org/10.1126/sciadv.aay0639>
- [23] Hui Jiang LL, Wang R, Han K, Wang Q (2021) Effects of chromium on the microstructures and mechanical properties of AlCoCr_xFeNi_{2.1} eutectic high entropy alloys. *Acta Metall Sinica* 34:1565–1573. <https://doi.org/10.1007/s40195-021-01303-4>. (English Letters)
- [24] Schuh B, Mendez-Martin F, Völker B, George EP, Clemens H, Pippan R, Hohenwarter A (2015) Mechanical properties, microstructure and thermal stability of a nanocrystalline CoCrFeMnNi high-entropy alloy after severe plastic deformation. *Acta Mater* 96:258–268. <https://doi.org/10.1016/j.actamat.2015.06.025>
- [25] Han Z, Ren W, Yang J, Tian A, Du Y, Liu G, Wei R, Zhang G, Chen Y (2020) The corrosion behavior of ultra-fine

- grained CoNiFeCrMn high-entropy alloys. *J Alloys Compd* 816:152583. <https://doi.org/10.1016/j.jallcom.2019.152583>
- [26] Stølen S, Ien SS, Grande T, Allan NL, Library WO (2004) *Chemical thermodynamics of materials: macroscopic and microscopic aspects*. Wiley
- [27] Lejček P (2010) *Grain boundary segregation in metals*. Springer, Heidelberg
- [28] Lejček P, Hofmann S (2019) Modeling grain boundary segregation by prediction of all the necessary parameters. *Acta Mater* 170:253–267. <https://doi.org/10.1016/j.actamat.2019.03.037>
- [29] Kaptay G (2016) Modelling equilibrium grain boundary segregation, grain boundary energy and grain boundary segregation transition by the extended Butler equation. *J Mater Sci* 51:1738–1755. <https://doi.org/10.1007/s10853-015-9533-8>
- [30] Kaptay G (2020) A coherent set of model equations for various surface and interface energies in systems with liquid and solid metals and alloys. *Adv Colloid Interface Sci* 283:102212. <https://doi.org/10.1016/j.cis.2020.102212>
- [31] Wynblatt P, Ku R (1977) Surface energy and solute strain energy effects in surface segregation. *Surf Sci* 65:511–531
- [32] Seah M, Hondros E (1973) Grain boundary segregation. *Proc R Soc London A Math Phys Sci* 335:191–212
- [33] White CL, Coghlan WA (1977) The spectrum of binding energies approach to grain boundary segregation. *Metall Trans A* 8:1403–1412. <https://doi.org/10.1007/BF02642853>
- [34] Černý M, Šesták P, Všianská M, Lejček P (2022) On agreement of experimental data and calculated results in grain boundary segregation. *Metals*. <https://doi.org/10.3390/met12081389>
- [35] Li L, Li Z, Kwiatkowski da Silva A, Peng Z, Zhao H, Gault B, Raabe D (2019) Segregation-driven grain boundary spinodal decomposition as a pathway for phase nucleation in a high-entropy alloy. *Acta Mater* 178:1–9. <https://doi.org/10.1016/j.actamat.2019.07.052>
- [36] Miracle DB, Miller JD, Senkov ON, Woodward C, Uchic MD, Tiley J (2014) Exploration and development of high entropy alloys for structural applications, *Entropy*. 16:494–525. <https://doi.org/10.3390/e16010494>
- [37] Erhart H, Grabke HJ (1981) Equilibrium segregation of phosphorus at grain boundaries of Fe–P, Fe–C–P, Fe–Cr–P, and Fe–Cr–C–P alloys. *Metal Sci* 15:401–408. <https://doi.org/10.1179/030634581790426877>
- [38] Lejček P, Šob M, Paidar V (2017) Interfacial segregation and grain boundary embrittlement: an overview and critical assessment of experimental data and calculated results. *Prog Mater Sci* 87:83–139. <https://doi.org/10.1016/j.pmatsci.2016.11.001>
- [39] Ustinovshikov YI (1984) Effects of alloying elements, impurities, and carbon on temper embrittlement of steels. *Metal Sci* 18:545–548. <https://doi.org/10.1179/030634584790419683>
- [40] Lejček P (1994) Characterization of grain boundary segregation in an Fe–Si alloy. *Anal Chim Acta* 297:165–178. [https://doi.org/10.1016/0003-2670\(93\)E0388-N](https://doi.org/10.1016/0003-2670(93)E0388-N)
- [41] Lejček P, Hofmann S (2016) Interstitial and substitutional solute segregation at individual grain boundaries of α -iron: data revisited. *J Phys Condens Matter* 28:064001. <https://doi.org/10.1088/0953-8984/28/6/064001>
- [42] Lejček P, Hofmann S (2008) Thermodynamics of grain boundary segregation and applications to anisotropy, compensation effect and prediction. *Crit Rev Solid State Mater Sci* 33:133–163. <https://doi.org/10.1080/10408430801907649>
- [43] Lejček P, Jäger A, Gärtnerová V (2010) Reversed anisotropy of grain boundary properties and its effect on grain boundary engineering. *Acta Mater* 58:1930–1937. <https://doi.org/10.1016/j.actamat.2009.11.036>
- [44] Hu C, Luo J (2022) Data-driven prediction of grain boundary segregation and disordering in high-entropy alloys in a 5D space. *Mater Horiz* 9:1023–1035. <https://doi.org/10.1039/D1MH01204E>
- [45] Gao MC, Gao P, Hawk JA, Ouyang L, Alman DE, Widom M (2017) Computational modeling of high-entropy alloys: structures, thermodynamics and elasticity. *J Mater Res* 32:3627–3641. <https://doi.org/10.1557/jmr.2017.366>
- [46] Lejček P, Hofmann S (1991) Segregation enthalpies of phosphorus, carbon and silicon at 013 and 012 symmetrical tilt grain boundaries in an Fe–3.5 at.% Si alloy. *Acta Metall Mater* 39:2469–2476. [https://doi.org/10.1016/0956-7151\(91\)90026-W](https://doi.org/10.1016/0956-7151(91)90026-W)
- [47] Cantwell PR, Frolov T, Rupert TJ, Krause AR, Marvel CJ, Rohrer GS, Rickman JM, Harmer MP (2020) Grain boundary complexion transitions. *Annu Rev Mater Res* 50:465–492. <https://doi.org/10.1146/annurev-matsci-081619-114055>
- [48] Rickman JM, Luo J (2016) Layering transitions at grain boundaries. *Curr Opin Solid State Mater Sci* 20:225–230. <https://doi.org/10.1016/j.cossms.2016.04.003>
- [49] Ferrari A, Körmann F (2020) Surface segregation in Cr–Mn–Fe–Co–Ni high entropy alloys. *Appl Surf Sci* 533:147471. <https://doi.org/10.1016/j.apsusc.2020.147471>
- [50] Zhao S (2021) Local ordering tendency in body-centered cubic (BCC) multi-principal element alloys. *J Phase Equilib Diffus* 42:578–591. <https://doi.org/10.1007/s11669-021-00878-w>
- [51] Turchanin M, Agraval P, Dreval L, Vodopyanova A (2021) Thermodynamics and chemical ordering of liquid Cu–Hf–Ni

- Ti-Zr Alloys. *J Phase Equilib Diffus* 42:623–646. <https://doi.org/10.1007/s11669-021-00898-6>
- [52] Yuan J, Liu Y, Li Z, Wang M, Wang Q, Dong C (2021) Cluster-model-embedded first-principles study on structural stability of body-centered-cubic-based Ti-Zr-Hf-Nb refractory high-entropy alloys. *J Phase Equilib Diffus* 42:647–655. <https://doi.org/10.1007/s11669-021-00899-5>
- [53] Chang LS, Rabkin E, Straumal B, Lejček P, Hofmann S, Gust W (1997) Temperature dependence of the grain boundary segregation of Bi in Cu polycrystals. *Scripta Mater* 37:729–735. [https://doi.org/10.1016/S1359-6462\(97\)00171-1](https://doi.org/10.1016/S1359-6462(97)00171-1)
- [54] Muschik T, Gust W, Hofmann S, Predel B (1989) The temperature dependence of grain boundary segregation in Ni In bicrystals studied with auger electron spectroscopy. *Acta Metall* 37:2917–2925. [https://doi.org/10.1016/0001-6160\(89\)90326-X](https://doi.org/10.1016/0001-6160(89)90326-X)
- [55] Prenosil B, Koutnik M, Mazanec K (1986) Preferential cosegregation and interaction of carbon with phosphorus in temper embrittlement. *Met Mater* 24:197–202
- [56] Liu G, Lu DH, Liu XW, Liu FC, Yang Q, Du H, Hu Q, Fan ZT (2019) Solute segregation effect on grain boundary migration and Hall-Petch relationship in CrMnFeCoNi high-entropy alloy. *Mater Sci Technol* 35:500–508. <https://doi.org/10.1080/02670836.2019.1570679>
- [57] Utt D, Stukowski A, Albe K (2020) Grain boundary structure and mobility in high-entropy alloys: a comparative molecular dynamics study on a $\Sigma 11$ symmetrical tilt grain boundary in face-centered cubic CuNiCoFe. *Acta Mater* 186:11–19. <https://doi.org/10.1016/j.actamat.2019.12.031>
- [58] Svoboda J, Fischer FD (2014) Abnormal grain growth: a non-equilibrium thermodynamic model for multi-grain binary systems. *Modell Simul Mater Sci Eng* 22:015013. <https://doi.org/10.1088/0965-0393/22/1/015013>
- [59] Mavrikakis N, Saikaly W, Mangelinck D, Dumont M (2020) Segregation of Sn on migrating interfaces of ferrite recrystallisation: quantification through APT measurements and comparison with the solute drag theory. *Materialia* 9:100541. <https://doi.org/10.1016/j.mtla.2019.100541>
- [60] Suhane A, Scheiber D, Popov M, Razumovskiy VI, Romaner L, Militzer M (2022) Solute drag assessment of grain boundary migration in Au. *Acta Mater* 224:117473. <https://doi.org/10.1016/j.actamat.2021.117473>
- [61] Tuchinda N, Schuh CA (2022) Grain size dependencies of intergranular solute segregation in nanocrystalline materials. *Acta Mater* 226:117614. <https://doi.org/10.1016/j.actamat.2021.117614>
- [62] Peng HR, Huo WT, Zhang W, Tang Y, Zhang S, Huang LK, Hou HY, Ding ZG, Liu F (2023) Correlation between stabilizing and strengthening effects due to grain boundary segregation in iron-based alloys: theoretical models and first-principles calculations. *Acta Mater* 251:118899. <https://doi.org/10.1016/j.actamat.2023.118899>
- [63] Gollapudi S, Soni AK (2020) Understanding the effect of grain size distribution on the stability of nanocrystalline materials: an analytical approach. *Materialia* 9:100579. <https://doi.org/10.1016/j.mtla.2019.100579>
- [64] Yifan Y, Wang Q, Lu J, Liu CT, Yang Y (2015) High-entropy alloy: challenges and prospects. *Mater Today*. <https://doi.org/10.1016/j.mattod.2015.11.026>
- [65] Vaidya M, Pradeep KG, Murty BS, Wilde G, Divinski SV (2017) Radioactive isotopes reveal a non sluggish kinetics of grain boundary diffusion in high entropy alloys. *Sci Rep* 7:12293. <https://doi.org/10.1038/s41598-017-12551-9>
- [66] Middleburgh SC, King DM, Lumpkin GR, Cortie M, Edwards L (2014) Segregation and migration of species in the CrCoFeNi high entropy alloy. *J Alloy Compd* 599:179–182. <https://doi.org/10.1016/j.jallcom.2014.01.135>
- [67] Wynblatt P, Chatain D (2019) Modeling grain boundary and surface segregation in multicomponent high-entropy alloys. *Phys Rev Mater* 3:054004. <https://doi.org/10.1103/PhysRevMaterials.3.054004>
- [68] Soto AO, Salgado AS, Niño EB (2020) Thermodynamic analysis of high entropy alloys and their mechanical behavior in high and low-temperature conditions with a microstructural approach—a review. *Intermetallics* 124:106850. <https://doi.org/10.1016/j.intermet.2020.106850>

Publisher's Note Springer Nature remains neutral with regard to jurisdictional claims in published maps and institutional affiliations.